Journal of Biomolecular Structure and Dynamics

ISSN: (Print) (Online) Journal homepage: www.tandfonline.com/journals/tbsd20

Biochemical and *in silico* analysis of the binding mode of erastin with tubulin

Gudapureddy Radha, Pratyush Pragyandipta, Pradeep Kumar Naik & Manu Lopus

To cite this article: Gudapureddy Radha, Pratyush Pragyandipta, Pradeep Kumar Naik & Manu Lopus (20 Feb 2024): Biochemical and *in silico* analysis of the binding mode of erastin with tubulin, Journal of Biomolecular Structure and Dynamics, DOI: 10.1080/07391102.2024.2317984

To link to this article: https://doi.org/10.1080/07391102.2024.2317984

JOURNAL OF BIOMOLECULAR STRUCTURE AND DYNAMICS
https://doi.org/10.1080/07391102.2024.2317984

Taylor & Francis
Taylor & Francis Group

RAPID COMMUNICATION

Biochemical and *in silico* analysis of the binding mode of erastin with tubulin

Gudapureddy Radha[a], Pratyush Pragyandipta[b], Pradeep Kumar Naik[b] and Manu Lopus[a]

[a]School of Biological Sciences, UM-DAE Centre for Excellence in Basic Sciences, University of Mumbai, Mumbai, India; [b]Department of Biotechnology and Bioinformatics, Center of Excellence in Natural Products and Therapeutics, Sambalpur University, Sambalpur, India

Communicated by Ramaswamy H. Sarma

ABSTRACT

Erastin (ERN) is a small molecule that induces different forms of cell death. For example, it has been reported to induce ferroptosis by disrupting tubulin subunits that maintain the voltage-dependent anion channels (VDACs) of mitochondria. Although its possible binding to tubulin has been suggested, the fine details of the interaction between ERN and tubulin are poorly understood. Using a combination of biochemical, cell-model and *in silico* approaches, we elucidate the interactions of ERN with tubulin and their biological manifestations. After confirming ERN's antiproliferative efficacy (IC_{50}, 20 ± 3.2 M) and induction of cell death in the breast cancer cell line MDA-MB-231, the binding interactions of ERN with tubulin were examined. ERN bound to tubulin in a concentration-dependent manner, disorganizing the structural integrity of the protein, as substantiated *via* the tryptophan-quenching assay and the aniline-naphthalene sulfonate binding assay, respectively. *In silico* studies based on molecular docking revealed a docking score of −5.863 kcal/mol, suggesting strong binding interactions of ERN with tubulin. Additionally, molecular dynamics simulation and Molecular Mechanics Poisson–Boltzmann Surface Area (MM-PBSA) analyses evinced the binding free energy ($\Delta G_{binding}$) of −31.235 kcal/mol, substantiating strong binding affinity of ERN with tubulin. Ligplot analysis showed hydrogen bonding with specific amino acids (Asn A226, Thr A223, Gln B247 and Val B355). QikProp-based ADME (absorption, distribution, metabolism and excretion) assessment showed considerable therapeutic potential for ERN.

Abbreviations: PDB: Protein Data Bank; OPLS: Optimized Parameters for Liquid Simulations; PRCG: Polak-Rebiere Conjugate Gradient; Glide XP_{Score}: Glide Score; E_{model}: Model energy score; GROMACS: GROningen MAchine for Chemical Simulations; MD Simulation: Molecular Dynamics Simulation; GTP: Guanosine triphosphate; GDP: Guanosine diphosphate; GAFF: General Amber Force Field; ACPYPE: AnteChamber PYthon Parser interface; NPT: The constant-temperature, constant-pressure ensemble; NVT: The constant-temperature, constant-volume ensemble; PME algorithm: Particle-mesh Ewald algorithm; RMSD: Root mean square deviation; RMSF: Root mean square fluctuation; Rg: Radius of gyration; $\Delta G_{bind,pred}$: Predicted binding free energy; MM-PBSA: Molecular Mechanics Poisson–Boltzmann Surface Area

ARTICLE HISTORY
Received 5 September 2023
Accepted 5 February 2024

KEYWORDS
Microtubules; tubulin; ferroptosis; erastin (ERN); molecular dynamics simulation

1. Introduction

Tubulin is a cytoskeletal protein with several critical cellular functions, including the orchestration of cell division, imparting structural stability to the cells and providing tracks for intracellular cargo movements (Schappi et al., 2014; Horio & Murata 2014). By guarding the mitochondrial channels, it regulates mitochondrial functions (Rostovtseva et al., 2008). Specifically, the voltage-dependent anion channels (VDACs) of mitochondria are guarded by tubulin, and tubulin-perturbing agents can disrupt crucial mitochondrial functions and promote different forms of cell death, including ferroptosis. With their ability to undergo selective stabilization, microtubules regulates the necessary and sufficient dynamicity and consequential functions of this cytoskeletal filament. Loss of optimum dynamicity can be harmful to the existence of cells.

Erastin (2-[1-[4-[2-(4-Chlorophenoxy)acetyl]-1-piperazinyl]ethyl]-3-(2-ethoxyphenyl)-4(3H)-Quinazolinone) is known to promote different forms of cell death. Once such cell death is ferroptosiswith features that differ from the classic programmed cell death, apoptosis (Dixon & Stockwell, 2019). Unlike apoptosis, for example, ferroptosis does not manifest membrane blebbing or caspase activation. It nevertheless exhibits mitochondrial damage, including loss of cristae, and lipid peroxidation (Li et al., 2018) (Dixon et al., 2012; Nirmala & Lopus, 2020). ERN is thought to facilitate this form of iron-dependent cell death by disrupting tubulin at the VDAC2 and VDAC3 of mitochondria (Yagoda et al., 2007; Maldonado et al., 2013;Dixon & Stockwell, 2014). However, how ERN interacts with tubulin is poorly understood. Here, using biophysical and cellular assays coupled with molecular docking

CONTACT Manu Lopus manu.lopus@cbs.ac.in School of Biological Sciences, UM-DAE Centre for Excellence in Basic Sciences, Vidyanagari, Mumbai, India.
Supplemental data for this article can be accessed online at https://doi.org/10.1080/07391102.2024.2317984.

and MD simulations, we report a tubulin-targeted mechanism of action of ERN.

2. Material and methods

2.1. Materials

Erastin (ERN), piperazine-N,N′-bis(2-ethanesulfonic acid) (Pipes), ethylene glycol tetraacetic acid (EGTA), magnesium sulfate ($MgSO_4$), guanosine-5′-triphosphate (GTP), 8-anilino-1-naphthalenesulfonic acid (ANS) and dimethyl sulfoxide (DMSO) were purchased from Sigma (St. Louis, MO). Bovine serum albumin (BSA), glutamate and Bradford reagent were from Himedia (Mumbai, India). All reagents used in the study were of analytical grade.

2.2. Cell culture, cell viability analyses and Western blot

MDA-MB-231 cells (a triple-negative breast cancer cell line; ATCC, Manassas, VA) were grown in Dulbecco's Modified Eagle's Medium (DMEM; Himedia, Mumbai, India). The media was supplemented with 10% fetal bovine serum and 1% penicillin-streptomycin (both from Himedia) in conducive culture conditions (humidified, 37 °C chamber containing 5% CO_2; Radha et al., 2022) provided by a Forma stericyle incubator (Thermo Fisher Scientific, Waltham, MA). For the cell viability assay, MDA-MB-231 cells were seeded at a density of 50,000/mL in a surface-treated 12-well plate and grew overnight. The cells were then exposed to different concentrations of ERN (0–40 μM) for 24–48 h. DMSO was used as the vehicle control. The IC_{50} concentration was then determined using a trypan blue dye-exclusion assay (Radha et al., 2022). For Western blot, cells were treated with ERN (20 μM) for different time periods (24 h and 48 h), harvested and lysed using a radioimmunoprecipitation assay buffer (RIPA buffer) with the following composition: 50 mM tris– HCl (pH 7.4), 150 mM NaCl, 0.1% (w/v) SDS, 0.5% (w/v) sodium deoxycholate and 1.0% (v/v) nonidet P-40. The samples were processed for electrophoresis and transferred onto a polyvinylidene fluoride membrane. We used 5% skimmed milk to block the membrane. The membrane was then incubated with the respective primary antibodies (GPX4 or GAPDH; 1:1000 dilution, Cell Signaling Technologies, Danvers, MA) at 4 °C overnight. Blots were then treated with horseradish peroxidase (HRP)-conjugated secondary antibodies for 4 h at 4 °C (1:1000, Cell Signaling Technologies). They were developed using chemiluminescent substrate (SuperSignal West Pico PLUS, MA, USA) obtained from Thermo Fisher Scientific, Waltham, MA, and scanned using ChemiDoc Touch (Bio-Rad, Hercules, CA).

2.3. Transmission electron microscopy (TEM)

The cells, after a 48-h treatment with the IC_{50} of ERN (20 μM) , were collected and fixed with 3% glutaraldehyde for 2 h at 4 °C. They were then washed with sodium cacodylate buffer (0.1 M) and dehydrated with different grades of alcohol. Araldite 'A' and Araldite 'B' treatments followed. An ultramicrotome (Leica UC7, Wetzlar, Germany) was used to cut ultrathin sections (70 nm). These thin sections were placed on copper grids (300 mesh), stained with lead citrate for 3 min, and visualized using a JEM 1400 Plus transmission electron microscope at 120 kV (JEOL, Tokyo, Japan).

2.4. Tubulin purification

Microtubule-associated proteins-free tubulin (MAP-free tubulin) was isolated from fresh goat brain with alternating cycles of temperature- and GTP-dependent assembly and dissassembly. PEM buffer (50 mM Pipes, 3 mM MgSO4, 1 mM EGTA and pH 6.8) was used for the isolation. The purified tubulin was aliquoted as 50 μL or 100 μL samples and stored at −80 °C until used (Guha et al., 1998).

2.5. Tryptophan-quenching assay

Different concentrations of ERN (0–125 μM) were incubated with tubulin (2 μM) in PEM buffer (45 min, 35 °C). A Tecan M200 Pro multimode reader (Tecan, Männedorf, Switzerland) was used for recording the spectra (excitation wavelength: 295 nm; emission wavelength range: 320–400 nm).

2.6. Anilino-naphthalene sulfonate (ANS)-binding assay

To study the effect of ERN on the tertiary structure of tubulin, an ANS binding assay was performed (Cheriyamundath et al., 2019). Breifly, purified tubulin (2 μM) was incubated with ERN (0–75 μM) for 30 min (35 °C; PEM buffer). After the incubation, the samples were treated with 50 μM ANS at 25 °C for 20 min in the dark. The samples were excited at 380 nm, and the emission spectra were measured (emission wavelength range, 420 nm–560 nm).

2.7. Computational modeling, molecular dynamics simulation and predicted ADME properties of ERN

From the protein data bank, the crystal structure (PDB ID: 6Y6D) of tubulin (2.20 Å resolution) was accessed. Using a multistep protein preparation program (Schrödinger, 2023), missing hydrogens were then added. Prime (Schrödinger, 2023) prediction tool allowed for the identification and repair of all missing side chain atoms. Finally, the protein structure was energy minimized using the micromodel (Schrödinger, 2023) with an energy gradient of 0.01 Kcal/mol. ChemDraw (ChemDraw_ V-22.0.0.22, 2022), was used to draw the molecular structure of ERN, followed by energy minimization using a macromodel (Schrödinger, 2023) using an Optimized Parameters for Liquid Simulations (OPLS 2005) as force field with an energy gradient of 0.001 kcal/mol. The Polak-Rebiere Conjugate Gradient (PRCG) algorithm was used for the energy minimization of the protein and the ligand. Further, the energy-minimized structure of ERN was geometrically optimized using Jaguar (Schrödinger, 2023), as reported earlier (Pragyandipta et al., 2023). Ligprep (Schrödinger, 2023) was used to develop multiple confirmations of ERN. Since the co-crystal structure of tubulin-bound ERN was not

available, we applied a blind docking approach to elucidate the putative binding site of ERN on tubulin and calculated its binding affinity. In this context, we have predicted several binding regions using SiteMap (Schrödinger, 2023). The binding sites with site scores $\geq$0.80 Å and a high degree of confidence and druggability were chosen, and the rest were considered insignificant and false-positive binding sites (Halgren, 2007, 2009). The grid boxes for different binding regions were created by the Glide grid receptor generation tool (Schrödinger, 2023). In general, two grid boxes were generated. An outer grid box of size 20 Å × 20 Å × 20 Å was generated to accommodate all the ligand atoms of a valid pose, and an inner grid box of size 12 Å × 12 Å × 12 Å was generated at the midpoint of the binding site. Glide XP (extra precision) (Schrödinger, 2023) was employed for docking. Of the 10,000 poses generated the Glide XP docking alogorithm, 1000 were used for energy minimization (1000-step conjugate gradients; dielectric constant, 4.0). The lowest energy conformations thus generated were evaluated for the docking scores. The scale factor of 0.4 for van der Waals raddi was applied to atoms of protein with absolute partial charges less than or equal to 0.25. Afterwards, 100 poses per ligand were generated. The best docked structure was then chosen based on the Glide Score (Glide XP_{Score}) function (Friesner et al., 2004; Halgren et al., 2004; Su et al., 2019). Glide XP_{score} is a more advanced variant of ChemScore (Eldridge et al., 1997) with components focused on force fields and additional terminology that account for solvation and repulsive interactions. Model energy score (E_{model}) was used to combine the energy grid score, Glide score and the ligands internal starin, to select the best pose.

The docked pose with the lowest docking score was further used for MD simulation of 100 ns by GROMACS 2019.2 (Groningen, The Netherlands) (Abraham et al., 2015) in the presence of GDP, GTP and magnesium, as per the methodology mentioned earlier (Pragyandipta et al., 2023). To acquire the topology and coordinates the protein was processed in GROMACS 2019.2 version using Amber99SB force field (Hornak et al., 2006). For the ligands (GTP, GDP and ERN) the parameters were determined by using General Amber force field (GAFF) (Wang et al., 2004) in the antechamber program of Amber 18 and the atomic point charges were properly assigned by AM1-BCC charge model (Jakalian et al., 2002). For building the small molecule topology and internal coordinates the tleap tool of Amber 18 and ACPYPE was used (Sousa da Silva & Vranken, 2012). In a truncated octahedron box with a distance of 12 Å between the walls of the box and atoms of the protein and TIP3P as a water model the complex solvation was done (Kumar Pedapati et al., 2023). Counterions having a physiological ionic strength of 0.15 M were used to balance the system. Further to remove any conflicting contacts a steepest descent approach of 10,000 steps was considered for energy minimization. For both protein and ligand, a position restriction of 10 kcal/Å^2 was applied. At first a 500 ps of NVT equilibration was run at 300 K followed by NPT equilibration of 500 ps, keeping the Parrinello–Rahman barostat at a reference pressure of 1 bar. Post equilibration a 100 ns of simulation with 2fs time step was done. The particle-mesh Ewald (PME) algorithm was used to study the long-range electrostatic interactions. Short-range electrostatic and van der Waals cutoffs were kept at 10 Å. The Shake algorithm limited the bonds (Ryckaert et al., 1977), while the modified Berendsen thermostat regulated the system temperature. The sequential snapshots of the atomic coordinates were captured every 20 ps. The root mean square deviation (RMSD), root mean square fluctuation (RMSF) and radius of gyration (Rg) were plotted. The RMSD calculation was computed as a function of time in respect to reference structure using the following formula:

$$RMSD(t) = \left[\frac{1}{M}\sum_{i=1}^{N} m_i \left|\mathbf{r}_i(t) - \mathbf{r}_i^{ref}\right|^2\right]$$

Here $M = \Sigma_i\, m_i$ and $r_i(t)$ is the position of atom **i** at time **t** after least square fitting the structure to the reference structure (r_i^{ref}) while r_i is the set of co-ordinates of the same atom but belongs to the structure that is being compared with the reference.

The RMSF calculation was done based on the formula:

$$RMSF_i = \left[\frac{1}{T}\sum_{t_j=1}^{T} \left|\mathbf{r}_i(t_j) - \mathbf{r}_i^{ref}\right|^2\right]$$

Here, ***T*** is the time over which one wants to average and $\mathbf{r_i^{ref}}$ is the reference position of particle *i*. Where this reference position was time-averaged postioned of the same particle ***i,*** i.e., $\mathbf{r_i^{ref}} = \boldsymbol{r_i}$.

The predicted binding free energy ($\Delta G_{bind,\ pred}$) of ERN with tubulin was determined using the Molecular Mechanics Poisson–Boltzmann Surface Area (MM-PBSA) (Kollman et al., 2000). Of 500 snapshots were extracted from the trajectory of the MD simulation for the last 10 ns with a time interval of 20 ps, and using the g_mmpbsa tool (Kumari et al., 2014), the $\Delta G_{bind,\ pred}$ was calculated.

Further, the Qikprop (Schrödinger, 2023) module was used to determine the ADME properties for ERN. Out of the total 44 parameters, properties with zero values were excluded. The suitability of the drug as a vital drug is evaluated in this module based on Lipinski's rule of five. When the molecule ignores this rule, it is supposed to exhibit decreased absorption or less permeability (Pragyandipta et al., 2023).

3. Results

3.1. Inhibition of cell viability and induction of ferroptosis by ERN

The antiproliferative effect of ERN (Figures 1(A,B)) on MDA-MB-231 breast cancer cells was measured by counting the number of cells in treated and untreated samples (trypan-blue dye exclusion assay). ERN inhibited cell viability in a dose-dependent fashion. For example, 10 μM, 20 μM and 30 μM ERN inhibited the cell viability by 20%, 50% and 60%, respectively, yielding an IC_{50} (half-maximal inhibitory concentration) value of 20 ± 3.2 μM after 24 h of incubation. The IC_{50} was slightly higher (22 ± 2.2 μM) after 48 h of drug exposure (Figure 1(B)). Next, the type of cell death induced by ERN was investigated. ERN reduced the expression of GPX4 in a

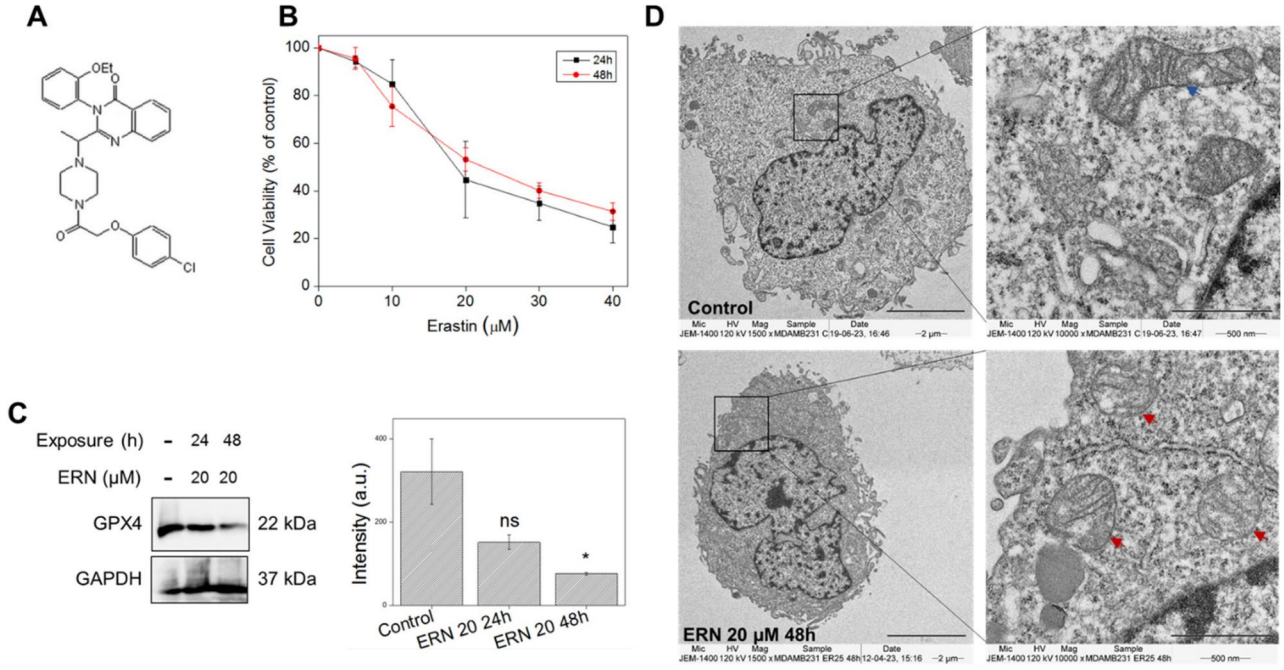

Figure 1. A. Structure of ERN and effects of ERN on MDA-MB-231 cells B. Inhibition of cell viability after 24 and 48 h incubation with ERN (0–40 μM) ($n = 3$) C. Western immunoblot showing GPX4 expression following ERN treatment (0, 20 μM; 24 h, 48 h). GAPDH served as loading control ($n = 3$). D. Electron micrographs of ERN-treated MDA-MB-231 cells showing distinctive morphological features of ferroptosis as compared to control.

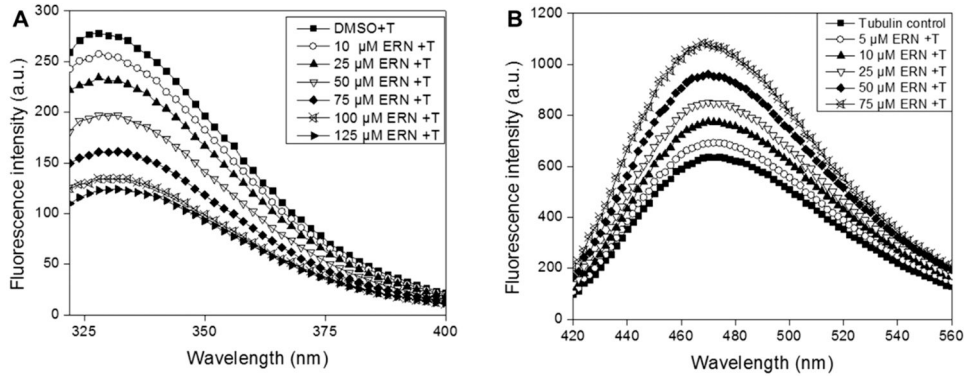

Figure 2. Interactions of ERN with tubulin and its effect on microtubules *in vitro* and in cells A. Dose-dependent binding of ERN to tubulin, as indicated by the reduction of intrinsic tubulin tryptophan fluorescence (*T*, tubulin). B. Dose-dependent enhancement of tubulin-ANS fluorescence by ERN, indicating perturbation of the tertiary structure of the protein. The spectra represent one of at least three independent experiments.

time-dependent manner (Figure 1(C)). For example, 20 μM ERN reduced the expression of GPX4 by 75% at 48 h of treatment, substantiating the induction of ferroptosis. The ultrastructure of ERN-treated cells, when visualized using TEM, further indicated ferroptosis (Figure 1(D)). Specifically, compared to the control cells, swollen mitochondria with considerable loss of cristae and rupturing of the outer mitochondrial membrane- some of the reported features associated with ferroptosis – were observed (Figure 1(D)).

3.2. Interactions of ERN with purified tubulin

We first investigated the ability of ERN to bind to purified tubulin using a tryptophan-quenching assay. A concentration-dependent reduction of the tryptophan fluorescence was observed, indicating the binding of ERN to the protein (Figure 2(A)). Specifically, 25 μM, 50 μM and 100 μM of ERN reduced the fluorescence by 19%, 27% and 39%, respectively, in comparison with the vehicle- treated control. The effect of ERN interactions on the tertiary structure of tubulin was assessed with an ANS-binding assay. The compound enhanced tubulin-ANS complex fluorescence with increasing ERN concentration (Figure 2(B)). Compared to the control sample, 10 μM, 25 μM and 50 μM, of ERN increased tubulin-ANS fluorescence by 21%, 28% and 41%, respectively, suggesting considerable perturbations in the tertiary structure of the protein.

3.3. Molecular docking, molecular dynamic simulation and predicted ADME properties of ERN

The blind docking approach was used to identify the most potent binding region for ERN with tubulin. All the predicted binding regions were evaluated for binding of ERN with tubulin and their binding affinity was evaluated using was Glide XP_{Score} (Friesner et al., 2004; Halgren et al., 2004; Su

Table 1. Docking result of ERN with tubulin against all the predicted binding sites.

Site ID	Site score (Å)^3	Volume (Å)^3	Dscore (Å)^3	Glide XP_{score} (Kcal/mol)	Glide Evdw (Kcal/mol)	Glide Emodel (Kcal/mol)	Glide Ecoul (Kcal/mol)	Glide Lipo (Kcal/mol)
1	1.006	848.196	1.018	−4.373	−53.86	−74.21	0.772	−5.623
2	1.086	599.65	1.091	−5.863	−49.864	−81.266	−12.367	−5.639
3	0.997	637.808	0.912	−5.025	−49.114	−78.311	−6.467	−3.125
4	1.049	324.392	1.054	−0.693	−44.407	−61.553	−1.035	−3.933
5	1.035	452.16	0.940	−5.465	−58.791	−72.077	0.129	−5.217
6	1.079	381.759	1.032	−4.351	−50.957	−77.48	−5.592	−4.476
7	0.980	268.483	0.987	−3.800	−36.277	−50.386	−6.628	−2.208
8	0.941	255.192	0.975	−5.813	−48.076	−78.178	−7.605	−5.381
9	0.975	159.752	0.953	−3.05	−40.914	−56.667	−3.873	−4.206
10	0.902	280.788	0.903	−4.311	−42.305	−78.983	−14.138	−2.928
11	0.915	152.635	0.852	−2.177	−23.514	−47.669	−8.201	−1.554
12	0.955	141.402	0.949	−3.136	−42.48	−64.735	−7.015	−3.33
13	1.040	191.137	0.853	−4.042	−43.423	−68.166	−7.537	−4.266
14	0.859	128.325	0.843	−3.786	−30.551	−50.876	−4.219	−3.06
15	0.984	112.118	0.946	−4.256	−41.293	−55.469	−4.33	−3.593

The Site ID 2, at the interface of α- and β-tubulin showed the lowest docking score, suggesting the potential binding site of ERN.

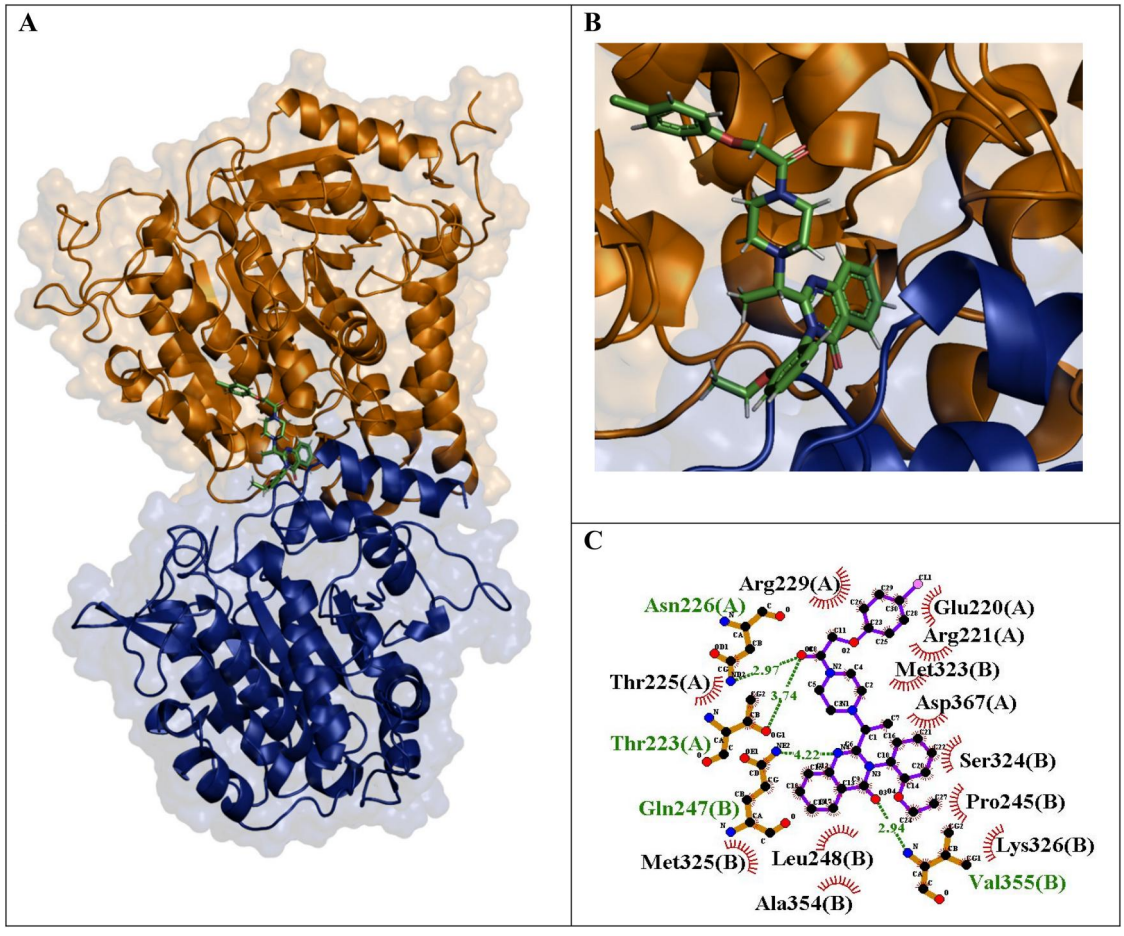

Figure 3. The binding mode of ERN with tubulin. A. ERN (green) is well accommodated inside the binding site at the interface of α- and β-tubulin. B. The binding site is represented as a macromodel surface according to α- (brown) and β-(blue) tubulin. C. 2D illustration of the interaction between the binding site residues and ERN. Dashed lines are the hydrogen bonds with their lengths being shown in Å. Hydrophobic interactions are represented by arcs with radial spokes. The figure was created using LIGPLOT (Wallace et al., 1995). Only the residues within 5 Å of the docked ligands are shown in the figures.

et al., 2019) function and docking scores are collated in Table 1. ERN showed considerably strong binding to tubulin at the interface of α- and β-subunits, with the lowest docking score value of −5.863 Kcal/mol (Table 1). This site was identified as the potential binding site for ERN (Figure 3(A,B)). The binding mode of ERN with tubulin (within 5Å) was visualized using Ligplot (Wallace et al., 1995) (Figure 3(C)). The ERN binding involved four hydrogen bonds with the residues of tubulin, Asn A226, Thr A223, Gln B247 and Val B355 (Figure 3(C)). Moreover, the interactions of ERN with the binding site residues showed a substantial amount of hydrophobic interaction (Supplementary Table S1). The stability of the ERN-tubulin co-complex throughout the 100 ns MD simulation was elucidated based on the RMSD, Rg

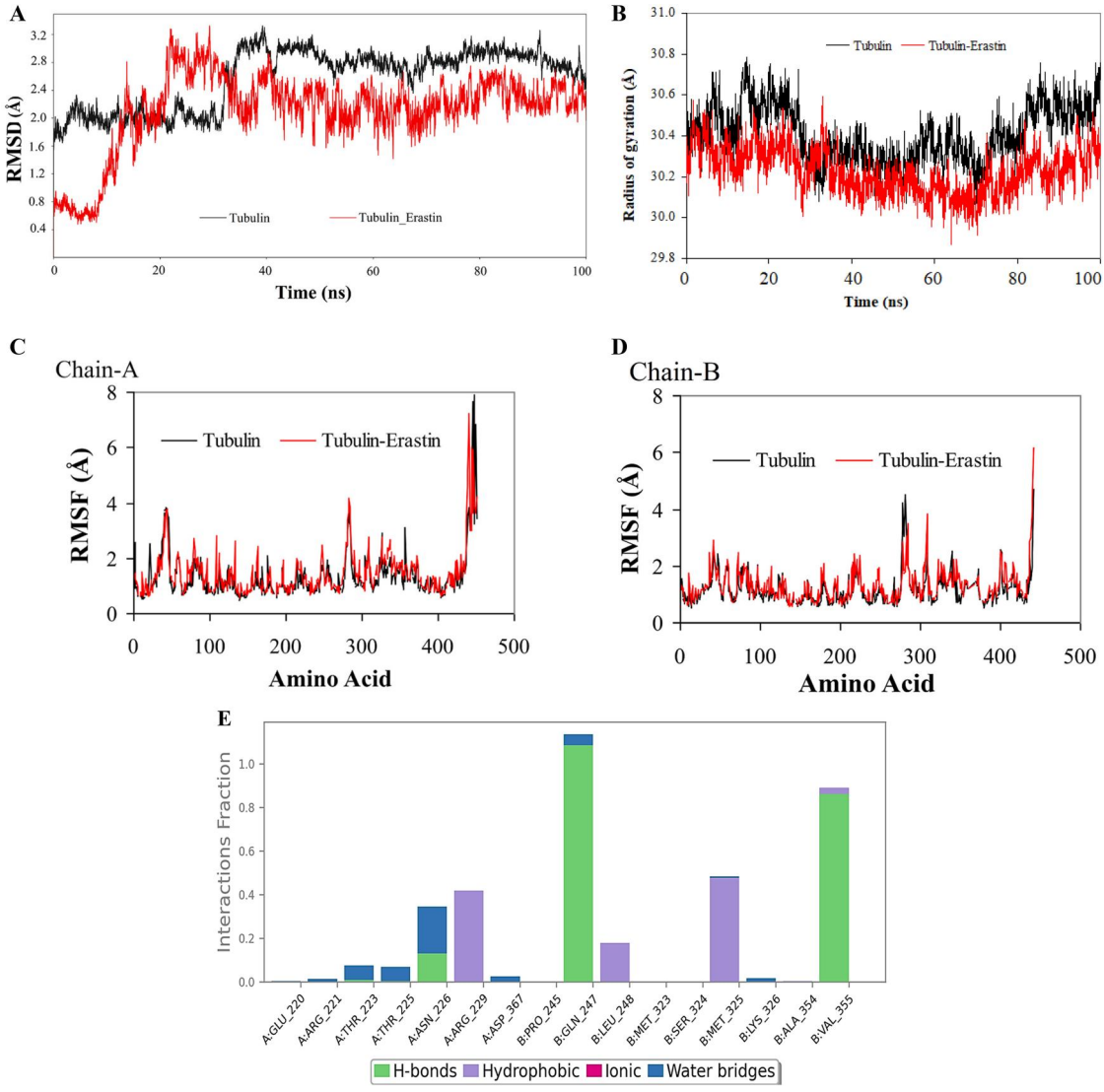

Figure 4. RMSD, radii of gyration and RMSF of the residues of tubulin in both free and ERN-bound state. RMSD (A) and radius of gyration of Cα carbon atoms (B) of tubulin only and in complex with ERN during MD simulation (100 ns). The RMSD and Rg of the Cα atoms showed only minor relative variations in the simulation, suggesting the complex's stability. C and D. RMSF of the tubulin amino acid residues in both the bound and unbound states with ERN. The flexibility level of the residues differed within the tubulin's free and ligand bounds forms. A minimal variability was exhibited by the amino acids, confirming that the residues are quite rigid in both the free and bound form of tubulin. E. Bar graph of protein-ligand contacts and interactions of ERN with binding site amino acids (H-bonds, hydrophobic, ionic and water bridges).

Table 2. Binding free energy along with its components (kcal/mol) for tubulin and ERN binding.

Complex	ΔE_{vdw} (kcal/mol)	ΔE_{ele} (kcal/mol)	$\Delta G_{SOL\text{-}PB}$ (kcal/mol)	$\Delta G_{SOL\text{-}NP}$ (kcal/mol)	$\Delta G_{bind\text{-}PBSA}$ (kcal/mol)
Tubulin_ERN	−28.541	−14.749	17.044	−4.989	−31.235

and RMSF plots. The low variation of RMSD (1.6–2.6 Å) and Rg (30–30.5 Å) values of the backbone C_α atoms was found to be quite minimal suggesting stability of the system (Figure 4(A,B)). The RMSF of the tubulin (Figure 4(C,D)) was analyzed to determine the flexibility of amino acids in both free form and ligand-bound form and the mean RMSF values for the contacting residues were found to be 0.68 Å and showed very little fluctuation (<4.0 Å) depicting the rigidness in both free and bound form. The Protein-ligand-contact mapping analysis revealed interactions of several amino acids with ERN like Glu 220, Arg 221, Thr 223, Asn 226, Arg 229, Asp 367, Pro 245, Gln 247, Leu 248, Met 323, Ser 324, Met 325, Lys 326, Ala 354 and Val 355 (Figure 4(E)). The 3D superimposition of the tubulin-ERN complex obtained during molecular docking and after MD simulation revealed RMSD of 2.494 Å (Supplementary Figure S1).

The predictive binding free energy ($\Delta G_{bind,PBSA}$) of ERN-tubulin is represented in Table 2 based on the MM-PBSA technique. The binding free energy was calculated by taking an average of 500 sequential snapshots acquired through the converged protein-ligand interactions complex of the last 10 ns of the MD simulation. ERN showed a stronger binding affinity with tubulin, with a $\Delta G_{bind,PBSA}$ value of −31.235 kcal/mol. The major contributors were the intermolecular van der Waals (ΔE_{vdw}) and electrostatic (ΔE_{ele}) interactions. They provided an energy contribution of −28.541 kcal/mol and −14.749 kcal/mol, respectively. In contrast, the polar solvation terms ($\Delta G_{SOL\text{-}PB}$) counteract binding. The non-polar

Table 3. ADME properties. ERN qualified all the qualities required for a vital ADME screening.

Sl No.	ADME screening	Erastin	Recommended values
1	MW	547.05	130–725
2	SASA	857.65	300–1000
3	Accpt HB	10.50	2.0–20.0
4	QPpolrz	58.45	13.0–70.0
5	QPlogPoct	2.93	8.0–35
6	QPlogPw	16.52	4.0–45.0
7	QPlogPo/w	3.81	−2.0-6.5
8	QPlogHERG	−6.42	Below −5.0
9	QPPCaco	205.93	<25 poor >500 great
10	QPlogBB	−0.21	−3.0–1.2
11	QPPMDCK	480.10	<25 poor >500 great
12	QPlogKp	−3.01	−8.0 to −1.0
13	QPlogKhsa	−0.85	−1.5-1.5
14	Rule of five (no. of violations)	1.00	Maximum is 4

solvation term ($\Delta G_{SOL\text{-}NP}$), although marginal, contributed favorably to the binding.

Several parameters for the prediction of ADME were determined as reported earlier (Pragyandipta et al., 2023). The acceptability of ERN as a vital drug was determined based on the Lipinski's rule of five approaches. Remarkably, it was seen that ERN showed notable values for all the attributes analyzed and confirmed all the drug-like capabilities (Table 3).

4. Discussion

Erastin has been reported to antagonize tubulin at the VDACs of mitochondria to induce cell death. However, the mode of interaction of ERN with tubulin is poorly understood. In this study, we investigated the fine details of the interactions between ERN and tubulin. To begin with, we examined the antiproliferative efficacy of ERN against MDA-MB-231 breast carcinoma cells. These cells represent one of the most malignant forms of breast cancer that has limited treatment options. In our study, we found its IC_{50} to be ~20 μM (Figures 1(A,B)). After confirming the antiproliferative potential of the drug, we examined the nature of the binding of ERN with tubulin. There are a number of *in vitro* assays that can be employed to verify whether a drug molecule binds to tubulin and to gain insights into the nature of binding. Using tryptophan fluorescence as a probe, concentration-dependent alterations in the local environment of the tryptophan(s) of tubulin in the presence of increasing drug concentrations were observed (Figure 2(A)). The concentration-dependent progressive perturbation of the microenvironment of the tryptophan residue was verified from the emission spectra of tryptophan fluorescence. Several tubulin-binding agents are capable of disrupting the structural integrity of the protein (Oliva et al., 2020; Acharya et al., 2009). The tryptophan-quenching assay, although used to substantiate the binding of a ligand to tubulin, will not give additional insights into the nature of drug-induced perturbation of the protein. One well-established, classic analysis to study the structural perturbation of proteins is the ANS-binding assay. ANS is a fluorescent probe that enhances its fluorescence upon binding to exposed hydrophobic patches on proteins. Enhancement of ANS-tubulin fluorescence in a dose-dependent manner by ERN suggests its ability to disorganize the tertiary structure of the protein (Figure 2(B)). Using these two assays, we confirmed the binding of ERN to purified tubulin. Further, the molecular interaction and stability of binding of ERN with microtubules were studied based on molecular docking and MD simulation that showed promising interactions of ERN at the interface between α and β tubulin monomers (Figures 3 and 4). The theoretical binding affinity calculated using MM-PBSA revealed stronger binding of ERN with tubulin (Table 2). Tubulin is a verified drug target for a variety of diseases, including cancer (Choudhary et al., 2022). Several agents, such as derivatives of noscapine (Pradhan et al., 2017), pyrazole derivatives (Minu et al., 2016) and surface-functionalized gold nanoparticles (Nirmala et al., 2021), can cause tubulin dysfunction and cell death. Here we show evidence that agents that can induce different forms of cell death, such as ferroptosis, possess considerable antitubulin activity and ADME properties.

Acknowledgments

The authors thank Transmission Electron Microscope facility, ACTREC, Navi Mumbai.

Disclosure statement

No potential conflict of interest was reported by the author(s).

Funding

The authors thank UM-DAE Centre for Excellence in Basic Sciences and Host Institute for financial support

ORCID

Manu Lopus http://orcid.org/0000-0002-4829-3960

References

Abraham, M. J., Murtola, T., Schulz, R., Páll, S., Smith, J. C., Hess, B., & Lindahl, E. (2015). GROMACS: High performance molecular simulations through multi-level parallelism from laptops to supercomputers. *SoftwareX*, *1–2*, 19–25. https://doi.org/10.1016/j.softx.2015.06.001

Acharya, B. R., Choudhury, D., Das, A., & Chakrabarti, G. (2009). Vitamin K3 disrupts the microtubule networks by binding to tubulin: A novel mechanism of its antiproliferative activity. *Biochemistry*, *48*(29), 6963–6974. https://doi.org/10.1021/bi900152k

ChemDraw_ V-22.0.0.22. *CambridgeSoft corporation*, 875 Massachusetts Ave., Cambridge, MA 02139. (2022) http://www.camsoft.com/

Cheriyamundath, S., Mahaddalkar, T., Reddy Nagireddy, P. K., Sridhar, B., Kantevari, S., & Lopus, M. (2019). Insights into the structure and tubulin-targeted anticancer potential of N-(3-bromobenzyl) noscapine. *Pharmacological Reports*, *71*(1), 48–53. https://doi.org/10.1016/j.pharep.2018.09.002

Choudhary, S., Lopus, M., & Hosur, R. V. (2022). Targeting disorders in unstructured and structured proteins in various diseases. *Biophysical Chemistry*, *281*, 106742. https://doi.org/10.1016/j.bpc.2021.106742

Dixon, S. J., Lemberg, K. M., Lamprecht, M. R., Skouta, R., Zaitsev, E. M., Gleason, C. E., Patel, D. N., Bauer, A. J., Cantley, A. M., Yang, W. S., Morrison, B., 3rd., & Stockwell, B. R. (2012). Ferroptosis: An iron-

dependent form of nonapoptotic cell death. *Cell*, *149*(5), 1060–1072. https://doi.org/10.1016/j.cell.2012.03.042

Dixon, S. J., & Stockwell, B. R. (2014). The role of iron and reactive oxygen species in cell death. *Nature Chemical Biology*, *10*(1), 9–17. https://doi.org/10.1038/nchembio.1416

Dixon, S. J., & Stockwell, B. R. (2019). The hallmarks of ferroptosis. *Annual Review of Cancer Biology*, *3*(1), 35–54. https://doi.org/10.1146/annurev-cancerbio

Eldridge, M. D., Murray, C. W., Auton, T. R., Paolini, G. V., & Mee, R. P. (1997). Empirical scoring functions: I. The development of a fast empirical scoring function to estimate the binding affinity of ligands in receptor complexes. *Journal of Computer-Aided Molecular Design*, *11*(5), 425–445. https://doi.org/10.1023/a:1007996124545

Friesner, R. A., Banks, J. L., Murphy, R. B., Halgren, T. A., Klicic, J. J., Mainz, D. T., Repasky, M. P., Knoll, E. H., Shelley, M., Perry, J. K., Shaw, D. E., Francis, P., & Shenkin, P. S. (2004). Glide: A new approach for rapid, accurate docking and scoring. 1. Method and assessment of docking accuracy. *Journal of Medicinal Chemistry*, *47*(7), 1739–1749. https://doi.org/10.1021/jm0306430

Guha, S., Manna, T. K., Das, K. P., & Bhattacharyya, B. (1998). Chaperone-like activity of tubulin. *The Journal of Biological Chemistry*, *273*(46), 30077–30080. https://doi.org/10.1074/jbc.273.46.30077

Halgren, T. A., Murphy, R. B., Friesner, R. A., Beard, H. S., Frye, L. L., Pollard, W. T., & Banks, J. L. (2004). Glide: A new approach for rapid, accurate docking and scoring. 2. Enrichment factors in database screening. *Journal of Medicinal Chemistry*, *47*(7), 1750–1759. https://doi.org/10.1021/jm030644s

Halgren, T. (2007). New method for fast and accurate binding-site identification and analysis. *Chemical Biology & Drug Design*, *69*(2), 146–148. https://doi.org/10.1111/j.1747-0285.2007.00483.x

Halgren, T. A. (2009). Identifying and characterizing binding sites and assessing druggability. *Journal of Chemical Information and Modeling*, *49*(2), 377–389. https://doi.org/10.1021/ci800324m

Horio, T., & Murata, T. (2014). The role of dynamic instability in microtubule organization. *Frontiers in Plant Science*, *5*, 511. https://doi.org/10.3389/fpls.2014.00511

Hornak, V., Abel, R., Okur, A., Strockbine, B., Roitberg, A., & Simmerling, C. (2006). Comparison of multiple Amber force fields and development of improved protein backbone parameters. *Proteins*, *65*(3), 712–725. https://doi.org/10.1002/prot.21123

Jakalian, A., Jack, D. B., & Bayly, C. I. (2002). Fast, efficient generation of high-quality atomic charges. AM1-BCC model: II. Parameterization and validation. *Journal of Computational Chemistry*, *23*(16), 1623–1641. https://doi.org/10.1002/jcc.10128

Kollman, P. A., Massova, I., Reyes, C., Kuhn, B., Huo, S., Chong, L., Lee, M., Lee, T., Duan, Y., Wang, W., Donini, O., Cieplak, P., Srinivasan, J., Case, D. A., & Cheatham, T. E. (2000). Calculating structures and free energies of complex molecules: Combining molecular mechanics and continuum models. *Accounts of Chemical Research*, *33*(12), 889–897. https://doi.org/10.1021/ar000033j

Kumar Pedapati, R., Pragyandipta, P., Pranathi Abburi, N., Chirra, N., Kantevari, S., & Naik, P. K. (2023). Antiproliferative noscapinoids bearing an amidothiadiazole scaffold as apoptosis inducers: Design, synthesis and molecular docking. *Chemistry & Biodiversity*, *20*(2), e202201089. https://doi.org/10.1002/cbdv.202201089

Kumari, R., Kumar, R., & Lynn, A. (2014). g_mmpbsa–a GROMACS tool for high-throughput MM-PBSA calculations. *Journal of Chemical Information and Modeling*, *54*(7), 1951–1962. https://doi.org/10.1021/ci500020m

Li, Q. Q., Li, Q., Jia, J. N., Liu, Z. Q., Zhou, H. H., & Mao, X. Y. (2018). 12/15 lipoxygenase: A crucial enzyme in diverse types of cell death. *Neurochemistry International*, *118*, 34–41. https://doi.org/10.1016/j.neuint.2018.04.002

Maldonado, E. N., Sheldon, K. L., DeHart, D. N., Patnaik, J., Manevich, Y., Townsend, D. M., Bezrukov, S. M., Rostovtseva, T. K., & Lemasters, J. J. (2013). Voltage-dependent anion channels modulate mitochondrial metabolism in cancer cells: Regulation by free tubulin and erastin. *The Journal of Biological Chemistry*, *288*(17), 11920–11929. https://doi.org/10.1074/jbc.M112.433847

Minu, M., Singh, D., Mahaddalkar, T., Lopus, M., Winter, P., Ayoub, A. T., Missiaen, K., Tilli, T. M., Pasdar, M., & Tuszynski, J. (2016). Chemical synthesis, pharmacological evaluation and in silico analysis of new 2,3,3a,4,5,6-hexahydrocyclopenta[c]pyrazole derivatives as potential anti-mitotic agents. *Bioorganic & Medicinal Chemistry Letters*, *26*(16), 3855–3861. https://doi.org/10.1016/j.bmcl.2016.07.025

Nirmala, J. G., & Lopus, M. (2020). Cell death mechanisms in eukaryotes. *Cell Biology and Toxicology*, *36*(2), 145–164. https://doi.org/10.1007/s10565-019-09496-2

Nirmala, J. G., Rachineni, K., Choudhary, S., Hosur, V. R., & Lopus, M. (2021). Triphala polyphenols-functionalized gold nanoparticles impair cancer cell survival through induction of tubulin dysfunction. *Journal of Drug Delivery Science and Technology*, *61*, 102167. https://doi.org/10.1016/j.jddst.2020.102167

Oliva, M. A., Prota, A. E., Rodríguez-Salarichs, J., Bennani, Y. L., Jiménez-Barbero, J., Bargsten, K., Canales, Á., Steinmetz, M. O., & Díaz, J. F. (2020). Structural basis of noscapine activation for tubulin binding. *Journal of Medicinal Chemistry*, *63*(15), 8495–8501. https://doi.org/10.1021/acs.jmedchem.0c00855

Pradhan, S., Mahaddalkar, T., Choudhary, S., Manhcukonda, N., Nagireddy, P. R., Kantevari, S., & Lopus, M. (2017). Elucidation of the tubulin-targeted mechanism of action of 9-(3-pyridyl) noscapine. *Current Topics in Medicinal Chemistry*, *17*(22), 2569–2574. https://doi.org/10.2174/1568026617666170104150304

Pragyandipta, P., Pedapati, R. K., Reddy, P. K., Nayek, A., Meher, R. K., Guru, S. K., Kantevari, S., & Naik, P. K. (2023). Rational design of novel microtubule targeting anticancer drugs N-imidazopyridine noscapinoids: Chemical synthesis and experimental evaluation based on in vitro using breast cancer cells and in vivo using xenograft mice model. *Chemico-Biological Interactions*, *382*, 110606. https://doi.org/10.1016/j.cbi.2023.110606

Radha, G., Naik, P. K., & Lopus, M. (2022). In vitro characterization and molecular dynamic simulation of shikonin as a tubulin-targeted anticancer agent. *Computers in Biology and Medicine*, *147*, 105789. https://doi.org/10.1016/j.compbiomed.2022.105789

Rostovtseva, T. K., Sheldon, K. L., Hassanzadeh, E., Monge, C., Saks, V., Bezrukov, S. M., & Sackett, D. L. (2008). Tubulin binding blocks mitochondrial voltage-dependent anion channel and regulates respiration. *Proceedings of the National Academy of Sciences of the United States of America*, *105*(48), 18746–18751. https://doi.org/10.1073/pnas.0806303105

Ryckaert, J. P., Ciccotti, G., & Berendsen, H. J. (1977). Numerical integration of the cartesian equations of motion of a system with constraints: Molecular dynamics of n-alkanes. *Journal of Computational Physics*, *23*(3), 327–341. https://doi.org/10.1016/0021-9991(77)90098-5

Schappi, J. M., Krbanjevic, A., & Rasenick, M. M. (2014). Tubulin, actin and heterotrimeric G proteins: Coordination of signaling and structure. *Biochimica et Biophysica Acta*, *1838*(2), 674–681. https://doi.org/10.1016/j.bbamem.2013.08.026

Schrödinger. (2023). *LLC, NY, Schrödinger release 2023-2*. Schrödinger

Sousa da Silva, A. W., & Vranken, W. F. (2012). ACPYPE - AnteChamber PYthon Parser interfacE. *BMC Research Notes*, *5*(1), 367. https://doi.org/10.1186/1756-0500-5-367

Su, M., Yang, Q., Du, Y., Feng, G., Liu, Z., Li, Y., & Wang, R. (2019). Comparative Assessment of Scoring Functions: The CASF-2016 Update. *Journal of Chemical Information and Modeling*, *59*(2), 895–913. https://doi.org/10.1021/acs.jcim.8b00545

Wallace, A. C., Laskowski, R. A., & Thornton, J. M. (1995). LIGPLOT: A program to generate schematic diagrams of protein-ligand interactions. *Protein Engineering*, *8*(2), 127–134. https://doi.org/10.1093/protein/8.2.127

Wang, J., Wolf, R. M., Caldwell, J. W., Kollman, P. A., & Case, D. A. (2004). Development and testing of a general amber force field. *Journal of Computational Chemistry*, *25*(9), 1157–1174. https://doi.org/10.1002/jcc.20035

Yagoda, N., von Rechenberg, M., Zaganjor, E., Bauer, A. J., Yang, W. S., Fridman, D. J., Wolpaw, A. J., Smukste, I., Peltier, J. M., Boniface, J. J., Smith, R., Lessnick, S. L., Sahasrabudhe, S., & Stockwell, B. R. (2007). RAS-RAF-MEK-dependent oxidative cell death involving voltage-dependent anion channels. *Nature*, *447*(7146), 864–868. https://doi.org/10.1038/nature05859